Tectonophysics 627 (2014) 159–170

Contents lists available at ScienceDirect

Tectonophysics

journal homepage: www.elsevier.com/locate/tecto

3-D density structure under South China constrained by seismic velocity and gravity data

Yangfan Deng [a,b,*], Zhongjie Zhang [b], José Badal [c], Weiming Fan [a]

[a] Guangzhou Institute of Geochemistry, Chinese Academy of Sciences, Guangzhou, 510640, China
[b] State Key Laboratory of Lithospheric Evolution, Institute of Geology and Geophysics, Chinese Academy of Sciences, Beijing, 100029, China
[c] Physics of the Earth, University of Zaragoza, Pedro Cerbuna 12, 50009 Zaragoza, Spain

ARTICLE INFO

Article history:
Received 25 April 2013
Received in revised form 16 July 2013
Accepted 24 July 2013
Available online 2 August 2013

Keywords:
P-wave velocity
Bouguer gravity
3-D density model
Vp–density laws
South China

ABSTRACT

Until now the crustal structure of South China has been studied through 2-D seismic surveys. While informative, the results generated from these surveys cannot be easily interpreted from a regional outlook due to the sparse sampling of the area. In this paper, we have investigated the 3-D density structure of South China based on an integrated dataset, namely: P-wave velocities previously determined from seismic profiles and Bouguer gravity anomalies. The density structure is solved through a robust inversion of Bouguer anomalies with the help of Grav3D software, so that the results can be extended to zones lacking constraints or sufficient deep seismic coverage. The key issues arising from this density analysis shed new lights on South China, as: (1) The Moho depth extracted from the density model is consistent with the information supplied by deep seismic soundings. (2) The linearly increasing density below the eastern part of the Dabie orogenic belt, in a frame of low density at the bottom of the middle crust, is consistent with the speculated dome of relatively high P-wave velocity suggested by previous deep seismic soundings, and understood as a geophysical fossil of the continental collision/extrusion. (3) The Chenzhou–Linwu fault seems to be the southern transection of the boundary between the Yangtze and Cathaysia blocks constrained by our crustal density model. (4) Different laws formulated as linear relationships between seismic velocity and density allow distinguishing the tectonic units forming South China. These laws are the consequence of the crustal composition and temperature distribution.

1. Introduction

South China, lying in the southeast of Eurasian continent and bordering with the Philippine Sea plate to the east and the Indian plate to the west (Fig. 1), is a major tectonic unit belonging to the continental margin of eastern Asia (Li and Li, 2007; Liu et al., 2012; C. Wang et al., 2003; Q.S. Wang et al., 2003; Y.J. Wang et al., 2003). It contains three Triassic–Jurassic orogens: the Qinling–Dabie orogenic belt along its northern margin, which records the collision with the North China block; the Longmenshan belt along its northwestern margin, likely related to the lower crust flow in the Tibetan Plateau; and the South China fold belt, which has a broad northeastward tread (Deng et al., 2013; Li, 1994; Li and Li, 2007; Wang, 2009; Wang and Shu, 2012; Zhang et al., 2009c, Z.J. Zhang et al., 2011, 2013).

In the course of the last 90 years, substantial research has been made to study the geological features of South China, and also the seismic velocity structure and the geometry of the main crustal interfaces. All these valuable data were acquired after many works of geophysical prospecting involving deep seismic soundings (DSS), deep reflections and broadband seismic surveys undertaken across many parts of South China (Deng et al., 2011; Li et al., 2006; Xiong et al., 2009; Zhang et al., 2005; Z.J. Zhang et al., 2011; Zhao et al., 2013a,b). However, due to uneven datasets, both in quality and quantity, the overall knowledge of the geological basement and the structure of the crust remains rather poor, and the boundary between the Yangtze and Cathaysia blocks is still a subject that even today raises a lively debate. Moreover, seismic data alone do not provide sufficient information about the density structure of the medium because the P- and S-wave velocities are controlled by a high number of factors including composition, temperature and volatile content of the crust–upper mantle structure (Mooney and Kaban, 2010). Gravity data and subsequently density data provide valuable constraints on the physical state of the lithosphere that are complementary to the seismic data. For example, density variations within the crust and sublithospheric mantle often control the surface elevation (Mooney and Kaban, 2010). So much so that a better understanding of South China can be achieved using a 3-D inversion of gravity data that integrates existing geological and geophysical information, to extrapolate the results to poorly sampled regions and thus fill the existing information gap.

In order to obtain the density structure in South China and discuss the feasible boundary between the Yangtze and Cathaysia blocks, in this paper, based on the available data of gravity, we have studied the

* Corresponding author at: Guangzhou Institute of Geochemistry, Chinese Academy of Sciences, Guangzhou, 510640, China. Tel.: +86 010 82998345.
E-mail address: dengyangfan@mail.iggcas.ac.cn (Y. Deng).

0040-1951/$ – see front matter © 2013 Elsevier B.V. All rights reserved.
http://dx.doi.org/10.1016/j.tecto.2013.07.032

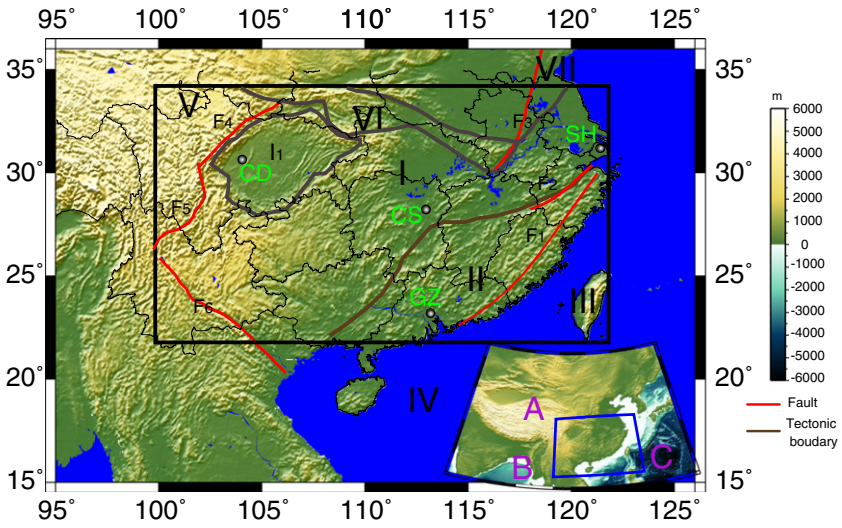

Fig. 1. Tectonic map of South China framed within the spatial window 100–122°E, 22–34°N. The inset in the bottom right corner shows the study area bounded by a rectangle. The elevation of the terrain (in meters) is indicated on the vertical scale on the right of the map. Faults (red lines) and tectonic boundaries (dark brown lines) are also drawn. Key to symbols: A, Asian plate; B, Indian plate; C, Philippine Sea plate; I, Yangtze block; II, Cathaysia block; III, Taiwan orogeny; IV, South China Sea basin; V, East of the Songpan–Ganzi block; VI, Qinling–Dabie orogen; VII, North China block; I1, Sichuan Basin; F1, Zhenghe–Dapu fault belt; F2, Jiangshan–Shaoxing fault belt; F3, Tanlu fault belt; F4, Longmenshan fault belt; F5, An'ninghe fault belt; F6, Honghe fault belt; CD, Chengdu City; CS, Changsha City; SH, Shanghai City; GZ, Guangzhou City.

area framed within the spatial window 100–122°E, 22–34°N (Fig. 1), taking into account a reference structural model constrained by P-wave velocity that was previously obtained by kriging interpolation from 57 DSS profiles (Deng et al., 2011). The so obtained results supply new insights about the geodynamics of South China.

2. Gravity data

The starting data of Bouguer gravity with reference to South China were taken from the Earth Gravitational Model 2008 (EGM2008) proposed by Pavlis et al. (2008, 2012), which provides information on a 2.5′ × 2.5′ sized grid displayed both inland and on the ocean, including synthetic gravity generated by GRACE and terrestrial gravity anomaly. The standard deviation of the field data is less than 5 mGal in the study region (Pavlis et al., 2008).

The Bouguer gravity sums all density changes due to the non-homogeneous structure of the crust caused by different geological formations, shallow deposits of materials and the undulation or dipping of the layers (Q.S. Wang et al., 2003; Zeng, 2005). In South China, small positive gravity anomalies (<100 mGal) are confined to regions near the coastal areas (Fig. 2). At a larger scale, small negative gravity anomalies (around −200 mGal) can be observed in part of the Qinling–Dabie orogen and Sichuan basin. In the Songpan–Ganzi block the Bouguer gravity increases progressively westward to more negative values reaching up to −550 mGal. Thus, it can be summarized that the higher the elevation of the terrain the lower the gravity anomaly. While, other direct information related to the faults and boundaries separating the tectonic units cannot be observed clearly in the study area.

3. Inversion for density structure

3.1. Implementation

The forward modeling of gravity involves computing the gravitational response from a prescribed density anomaly model. Conversely, the inversion for a density anomaly structure or inverse modeling implies generating a model that fits the observed gravitational field in the subsurface, even though the resulting model is non-unique and simply represents one of many models that can satisfy the observations (Welford and Hall, 2007; Welford et al., 2010).

The inverse problem was formulated as an optimization by which an objective function defining the density model is minimized subject to the constraints of that the data be reproduced within a tolerance interval or error margin (Wang, 2002). With the purpose of constructing a 3-D density model we performed a robust inversion of the data using Grav3D software, by controlling the generation of the model type and to what extent the inverted model can reproduce the observed data within their error bounds (misfit) (Welford and Hall, 2007). The first step is made through the norm of the model that is described in terms of directionally dependent smoothing length scales, which can generate a variety of model types (e.g. small, flat, blocky). The norm can be further adapted to minimize the difference between the inverted density model and a reference density model. The misfit is a least-squares measure of the difference between the observed gravity values and those predicted from the inverted density anomaly model. The difference is weighted by the reciprocal of the observed data errors so that the misfit for inversion is dimensionless and should be equal to the number of data points provided that the data errors are independent and Gaussian with zero mean (Li and Oldenburg, 1996, 1998).

It is well known that the gravity data have no inherent resolution at depth; as most they lead to structures located near the surface when considered a simple model, i.e. a small or flat model, regardless of the true depth of the causative bodies. Since the amplitude of the inversion kernels decreases rapidly with depth, the data measured at surface are not enough as to generate a function (a density model) able to reveal a significant structure at depth. In order to overcome this drawback, the inversion process needs to introduce a weighting at depth to counteract this natural decay of the inversion kernels. Intuitively, such a weighting will approximately cancel the natural decay and will make possible constructing the model at gradually increasing depths, with equal probability of including non-zero density data in the solution (Grav3D 3.0).

With the Grav3D algorithm, a specific density anomaly is initially assigned to each grid cell covering the reference density model, and also a variation range wherein the density anomaly is allowed to vary during the inversion process. This allows that portions of the reference model that are well constrained by other geophysical methods may vary slightly or even remain fixed during the inversion process (Welford et al., 2010).

The Grav3D mesh, onto which the 3-D density anomaly distribution is modeled, consists of rectangular prisms of certain size with a particular

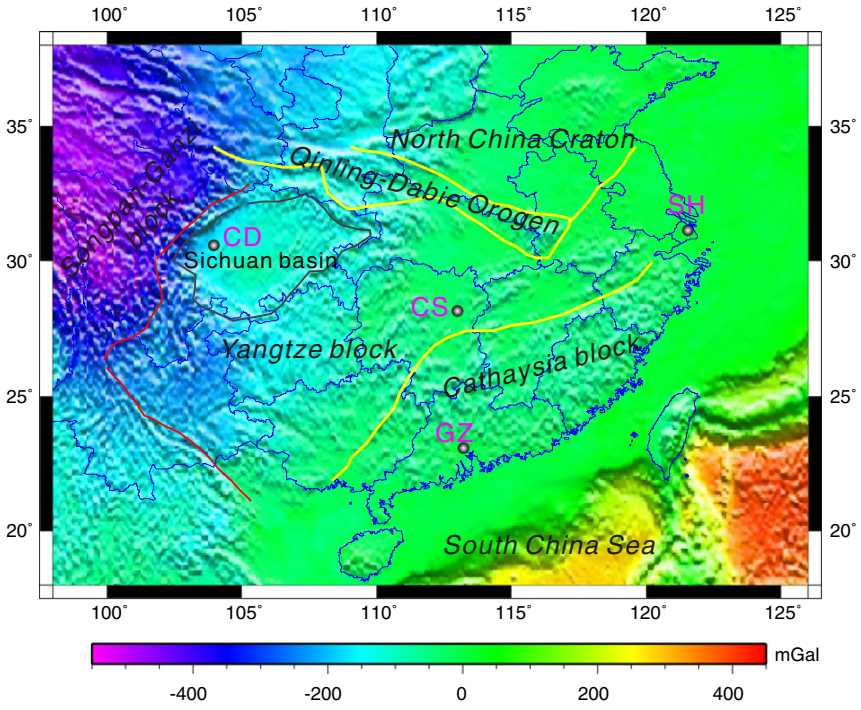

Fig. 2. Map of the Bouguer gravity anomaly in South China and adjacent regions. Again the main tectonic units appear clearly outlined (Fig. 1). Some important cities are also indicated as reference: CD, Chengdu City; CS, Changsha City; SH, Shanghai City; GZ, Guangzhou City. Small positive gravity anomalies (<100 mGal) are confined to regions near the coastal areas. At a larger scale, small negative gravity anomalies (around −200 mGal) can be observed in part of the Qinling–Dabie orogen and Sichuan basin. In the Songpan–Ganzi block the Bouguer gravity increases progressively westward to more negative values up to reach −550 mGal.

density anomaly assigned to each prism. In the present study, the mesh was constructed from cubes with base of 0.25° × 0.25° and height of 500 m. Given the study area (Fig. 1), the mesh is spatially composed of 97 cells in the horizontal direction x (coordinate in east longitude), 57 cells in the horizontal direction y (coordinate in north latitude) and 141 cells in the vertical direction z (coordinate in depth).

3.2. Reference model

The method requires a priori choice of a reference density model. The incorporation to this model of tighter constraints provided by other complementary studies can help the inversion process and finally generate a more realistic density model. The Bouguer gravity anomaly is generated by the undulation and variable density of the crustal layers. Basically, we took into account a horizontal homogeneous density model (HHDM) as prior information before gravity inversion. As is generally assumed, it is supposed that any change in HHDM would lead to a change in the value of the Bouguer gravity anomaly (Mooney and Kaban, 2010), since the gravitational effect of a layer with constant density and fixed boundaries is a constant value. HHDM describes a continental crust with flat topography, integrated by an upper layer of thickness 15 km that has a density of 2.7 g/cm^3 and a lower crust with density 2.94 g/cm^3 (Deng et al., 2011; Mooney and Kaban, 2010). The average density of the topmost upper mantle is set equal to 3.35 g/cm^3 (Mooney and Kaban, 2010). The Moho depth is set equal to 40 km, which is its average value in South China (Deng et al., 2011).

The initial density structure for inversion was defined from seismic velocity data acquired from 57 DSS performed in South China (Deng et al., 2011) and the relationship between P-wave velocity and density is given by Feng et al. (1986):

$$\rho = 2.78 + 0.56 * \left(v_\rho - 6.0\right); v_\rho \le 6.0 \quad (1)$$

$$\rho = 3.07 + 0.29 * \left(v_\rho - 7.0\right); 6.0 < v_\rho \le 7.5 \quad (2)$$

$$\rho = 3.22 + 0.20 * \left(v_\rho - 7.5\right); v_\rho \ge 7.5. \quad (3)$$

Fig. 3 shows this model where the seawater density is set as 1.05 g/cm^3. The method works with density anomalies, which are defined regarding HHDM. In other words: the 3-D density anomaly distribution is modeled by means of rectangular prisms whose respective density anomalies and sizes are taken as differences with respect to HHDM, so that the result we obtain by inversion is a density anomaly model, while the final density model (discussed later) is the density anomaly model plus HHDM.

3.3. Assessment of results

Regarding the Grav3D software itself, several studies have confirmed that it is able to recover the information from synthetic models (Cella et al., 2007; Dutra and Marangoni, 2009; Li and Yang, 2011); inverted density structures have been reported for the shallow structure of the Somma–Vesuvius volcano (Cella et al., 2007), Central Brazil (Dutra and Marangoni, 2009), North China (Li and Yang, 2011), the Newfoundland continental margin (Welford and Hall, 2007) and the Irish Atlantic continental margin (Welford et al., 2010). Using the density anomaly model as reference and the parameters outlined above, we obtained the 3-D density model doubly constrained by seismic velocities and gravity data that is shown in Fig. 4.

3.3.1. Uncertainty of the results

The fit between observed and computed gravity anomalies greatly supports the reliability of the results. The predicted Bouguer gravity anomalies as well as the differences between observed and calculated anomalies are shown in Fig. 5. This discrepancy (lower plot) rarely exceeds 10 mGal throughout the study region, its standard deviation is

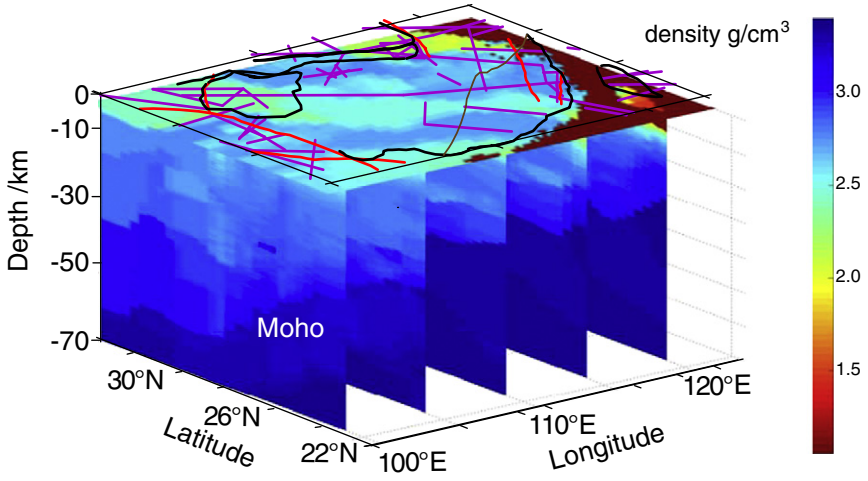

Fig. 3. Initial density model for South China as derived from P-wave velocity.

as small as 1.1 mGal, and there are no regional trends. So the density structure obtained by inversion allows us to successfully reproduce the gravity observations in South China. As can be seen, all the main gravity features seem to be well recovered and the gravity field values agree well with the observed ones, being the highest positive values close to 350 mGal, while the highest negative ones reach up to −550 mGal (Fig. 5a). As with the observed data (Fig. 2), the computed anomalies are generally positive in mainland, but negative in the marine areas.

A commonly used method in inverse problems is the generalized cross-validation (GCV) technique. If GCV mode is used, this misfit should be within the rough range 0.5 ∗ N–5.0 ∗ N, being N the number of data (Grav3D 3.0). In the present study we achieved a final misfit of 1.11481E + 04 with 5529 data, so the result is supposed to be a valid approximation to 3-D density.

Although the inversion provides a density model that recovers the long-wavelength information with success, the true is that short-wavelength perturbations still can be appreciated in the plot that shows the observation–calculation discrepancy (Fig. 5b). They are all a direct consequence of the blocky mesh parameterization and of imposing a strict limitation on the ocean water, and to a lesser extent of the sedimentary layers of the reference density model (Welford and Hall, 2007; Welford et al., 2010).

Other than the uncertainty of the relationship between P-wave velocity and density, and the unavoidable error inherent to the inversion problem, an additional error source could be the interpolation of data sampled from the numerous deep seismic soundings regarded from the beginning.

3.3.2. Moho undulation

Next we will assess the results by contrast with the Moho depth determined from deep seismic soundings. Since the 70s, the deep velocity structure of South China has been studied from 57 DSS profiles (Deng

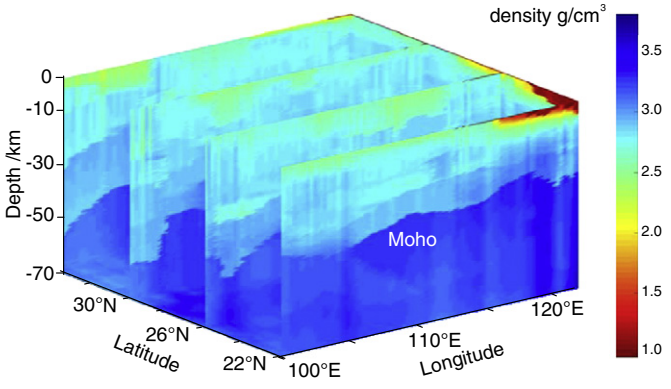

Fig. 4. Density model for South China as derived from inversion of the available data. Rectangular prisms were constructed from cubes with base of 0.25° × 0.25° and height of 500 m.

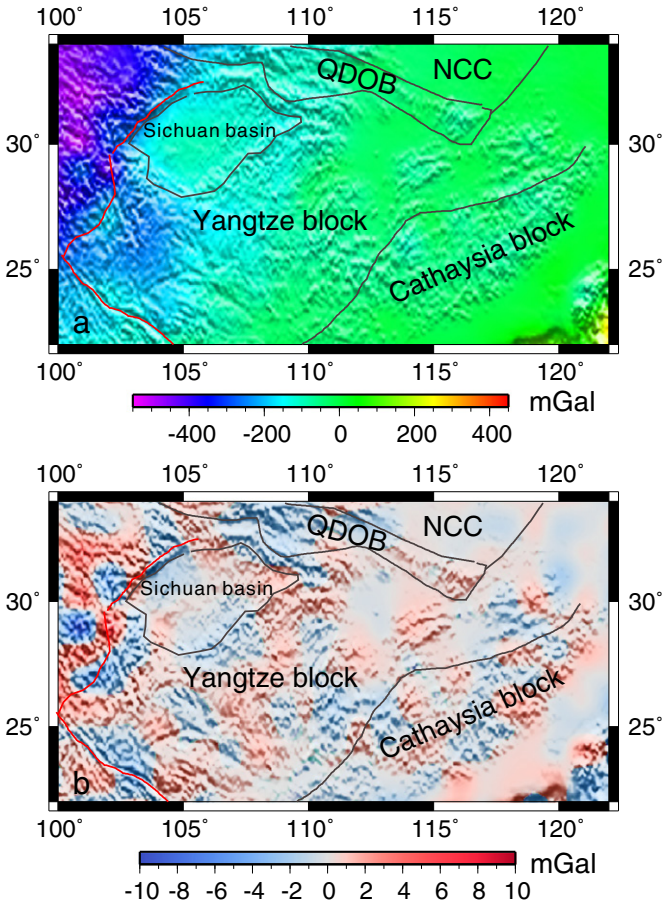

Fig. 5. (a) Predicted Bouguer gravity anomalies. (b) Differences between observed and calculated anomalies. QDOB: Qinling–Dabie orogen belt. This discrepancy rarely exceeds 10 mGal and its standard deviation is as small as 1.1 mGal.

et al., 2011). Among all of them, Fig. 6 shows five wide-angle reflection/refraction profiles: a) Zhubalong–Zizhong (C. Wang et al., 2003); b) Nanbu–Fushun (Cui et al., 1996); c) Zhuangmu–Anyi (Dong et al., 1998); d) Tunxi–Wenzhou (Zhang et al., 2005, 2008); e) Lianxian–Gangkou (Zhang and Wang, 2007; Zhang et al., 2009b; Zhao et al., 2013a). The Chinese Academy of Sciences (CAS), the China Earthquake Administration (CEA) and the Ministry of Land and Resources of China (MLR) contributed to perform these seismic profiles during the last 20 years. The Moho discontinuity marks the boundary between the crust and mantle, and generally the P-wave velocity value representing the crust–mantle transition is assumed to be 8.0 km/s (Teng, 2003; T. Xu et al., 2010; Y. Xu et al., 2010). Although the Moho interface is classically defined as a seismic velocity discontinuity, rather than as a specific density contrast, nonetheless an attempt to extract information on the Moho from a density anomaly model can be accomplished considering the density value 3.35 g/cm^3 as the one depicting the Moho discontinuity. Fig. 6 shows different density sections along the profiles mentioned above that allow to explore the Moho undulation. In section (a) the Moho depth decreases from west to east from 60 km to 40 km, and remains practically constant (about 42 km) in the Sichuan basin. The profile (b) supports this result, at the same time that reveals a relatively high density in the lower crust. In section (c) the Moho has a remarkable undulation beneath the Dabie orogen, which could be the result of the Mozitan fault and is consistent with the result derived from a deep seismic sounding (Liu et al., 2003). The overall thickness of the crust along the profile (d) decreases from 36 km beneath Tunxi in the northwest to 31 km beneath Wenzhou in the southeast. And in density section (e), the crust thickness gradually thins from northwest to southeast. The maximum depth of the crust is 34 km at Lianxian to the west and about 32 km at Gangkou to the east. The Moho topography along the Lianxian–Gangkou profile has a geometrical uplift below the middle transect (120–260 km) of the profile.

As shown in Fig. 6, compared to the depth given by deep seismic soundings, the Moho depth can be well delineated from the density structure obtained by inversion of Bouguer gravity data. In the present case, the results displayed in Fig. 6 seem to suggest that the crust is fairly compensated isostatically according to the Airy model in South China.

In summary, even though we cannot fully assess all the errors dragged so far, what we can say is the 3-D density model (Fig. 4) is a feasible model that provides a helpful image of the South China crust.

4. Discussion

4.1. Crustal density structure under the Dabie orogen

The Qinling–Dabie–Sulu orogenic belt in central-eastern China occupies a Triassic collision zone, between the Sino-Korean and Yangtze blocks (Hirajima and Nakamura, 2003), and is the largest high-pressure (HP) and ultra-high pressure (UHP) metamorphic zone in the world (Okay, 1993; Zheng, 2008; Zheng et al., 2003). Various wide-angle reflection/refraction profiles have enabled to study the Dabie orogen. It has been found that there is a high-velocity buried dome to the east of this unit (Bai et al., 2007; Dong et al., 1998; Liu et al., 2003). Also, high-resolution mantle tomography (Huang and Zhao, 2006) and other large-scale seismic studies (Ma and Zhou, 2007; Zheng et al., 2008) covering the Dabie orogen have been carried out; in particular, Luo et al. (2012) have studied the crustal structure beneath the Dabie orogenic belt from ambient noise tomography and have found high shear-wave velocities beneath the HP/UHP metaphoric zones at shallower depth than 9 km which corresponds to the top of the dome.

In order to discuss the crustal density response to the continent–continent collision between the North China Craton and the Yangtze Craton during the Triassic Period (Li, 1994; Li et al., 1993), in Fig. 7 we show several oblique density sections beneath the Dabie orogen that

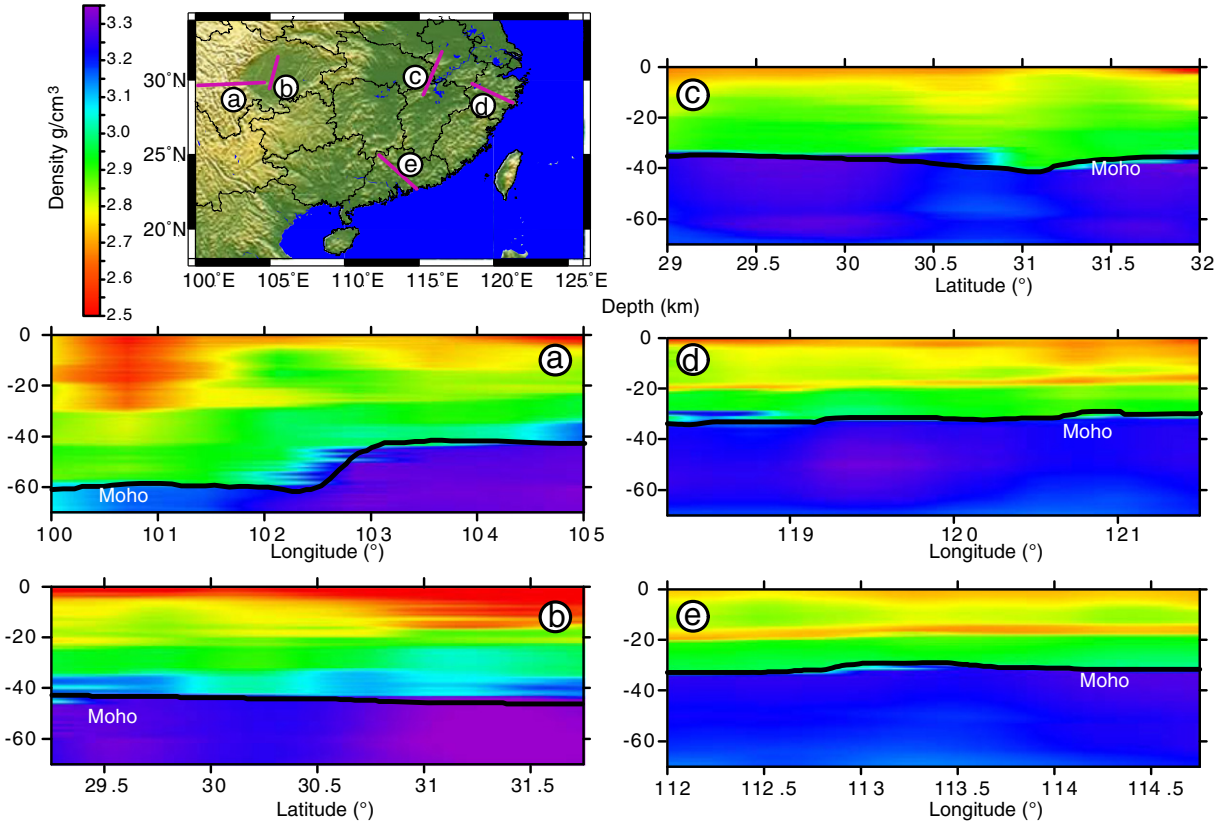

Fig. 6. Density sections along the profiles indicated (inset in the top left corner), all of them constructed from the previous density model: (a) Zhubalong–Zizhong, (b) Nanbu–Fushun, (c) Zhuangmu–Anyi, (d) Tunxi–Wenzhou and (e) Lianxian–Gangkou. The Moho discontinuity can be drawn quite well in comparison with the curve obtained from the results from wide-angle reflection/refraction profiles.

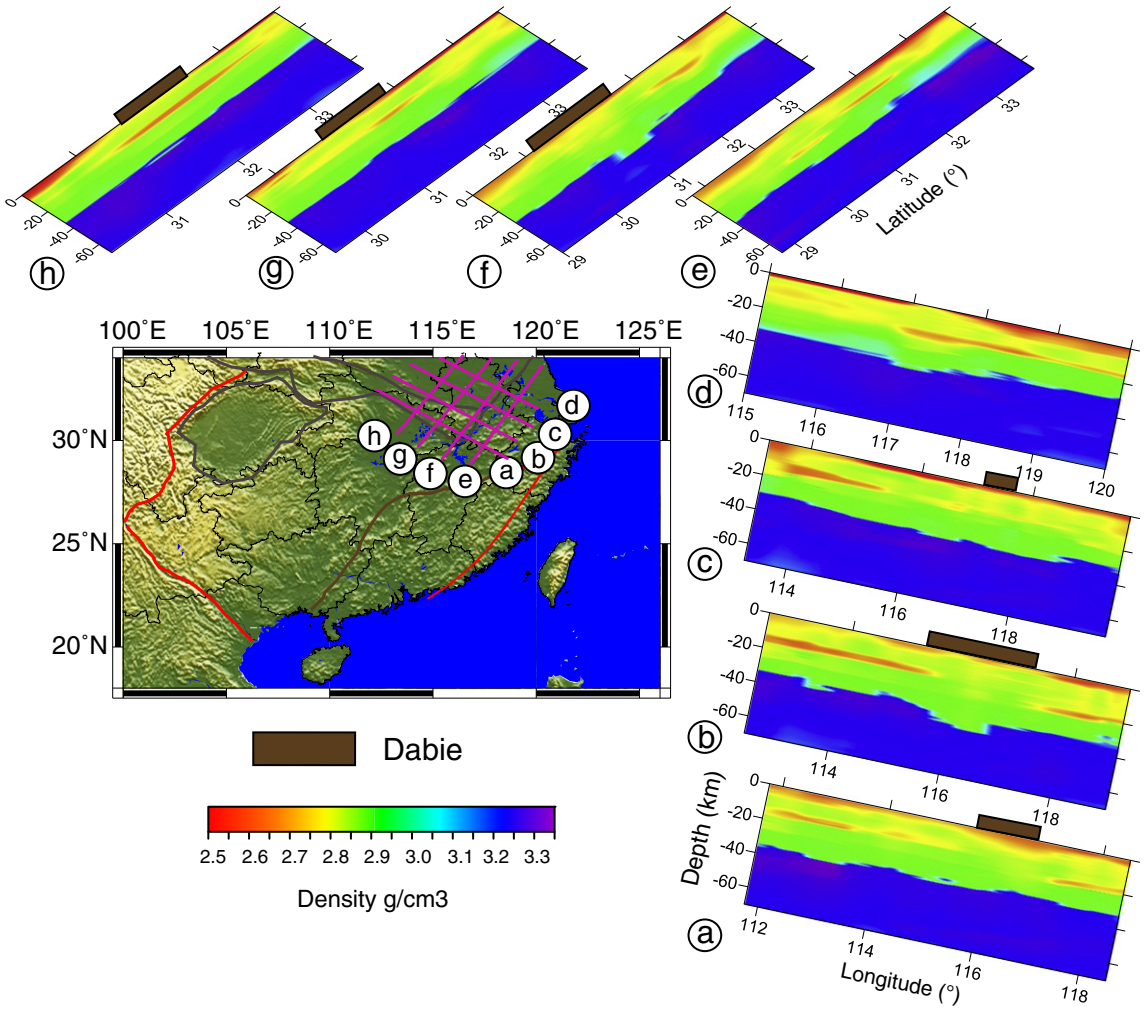

Fig. 7. The density structure beneath the Dabie orogen (zone marked on top of each profile) such as is deduced from this study. The sections make reference to the profiles labeled on the map of the study region (middle of the figure).

make reference to the profiles labeled on the map of the study region (middle part of Fig. 7). The existence of a low-density layer is more or less common in the 10–20 km depth range. However, such low density structure does not appear or is blurred beneath the east of Dabie, which is called buried dome including eclogite (Liu et al., 2003, 2005). The density dome could be the result from the collision between the North China Craton and the Yangtze Craton, and the low density beside it may play an important role in the post-collisional crust extension and exhumation of the ultra-high pressure metamorphic rocks (Dong et al., 1998; Liu et al., 2003).

Another important feature can be seen in the section shown in Fig. 7b: there is a remarkable elevation of the crustal layers and topography at longitude 116.5–117°N, and the Moho discontinuity also increases its depth at 115.5–117°N, which reflects the huge influence of the Tanlu fault between the South China block and the North China block (Deng et al., 2012).

4.2. The boundary between the Yangtze and Cathaysia blocks

The Phanerozoic tectonic regimes in South China are keys to understand the geodynamic evolution of the region with respect to the formation of abundant mineral resources (Y.J. Wang et al., 2003; Zhao et al., 2013b). It is well proved that the final formation of the South China block is due to the amalgamation of the Yangtze block to the northwest with the Cathaysia block to the southeast during the Neoproterozoic period (Y.J. Wang et al., 2003, 2012; Zhang et al., 2008). The Jiangshan–Shaoxing fault is generally considered as the north segment of the natural boundary between the Yangtze and Cathaysia blocks (Zhang et al., 2005, 2008; Zhao et al., 2013a,b) that are the two major tectonic units of southeastern China (Huang, 1977; Li, 1992). Such a distinction between regional blocks has been proposed on the basis of the age differences of low-grade metamorphic rocks (Wang and Qiao, 1984), occurrence of ophiolite suites (Zhang et al., 1984), stratigraphic records (Ji and Coney, 1985), differences in the lithology of the Precambrian basement (Granitoid Research Group of the Nanling Project, 1989); and more recently according to the observed dissimilarities in composition (Zhang et al., 2008), anisotropy (Zhang et al., 2009a), P-wave velocity (Zhang et al., 2009b, 2012) and S-wave velocity (Zhao et al., 2013a). But the standpoints about the boundary in the south part are still quite different. This issue is discussed henceforth.

Fig. 8 shows several possible cases wherein the borders under discussion separate different tectonic units in South China. These units are crossed from northwest to southeast by two shading narrow bands labeled ① and ②, that are two transects taken as reference later (in Figs. 9 and 10). There are mainly four kinds of views on this issue. The first is based on the geochemistry and geochronology of the area (Li et al., 2002, 2008; Liu et al., 2012; Wang et al., 2009) and postulates that the Chenzhou–Linwu fault is the boundary (hypothesis suggested in Fig. 8d). The basement rocks of the Yangtze block have an average age of 2.7–2.8 Ga, some of them even have an age >3.2 Ga (Qiu et al., 2000). In contrast, the basements of the Cathaysia block exhibit Paleo-to-Mesoproterozoic and possibly Late Archean ages of ~2.5 Ga (Chen

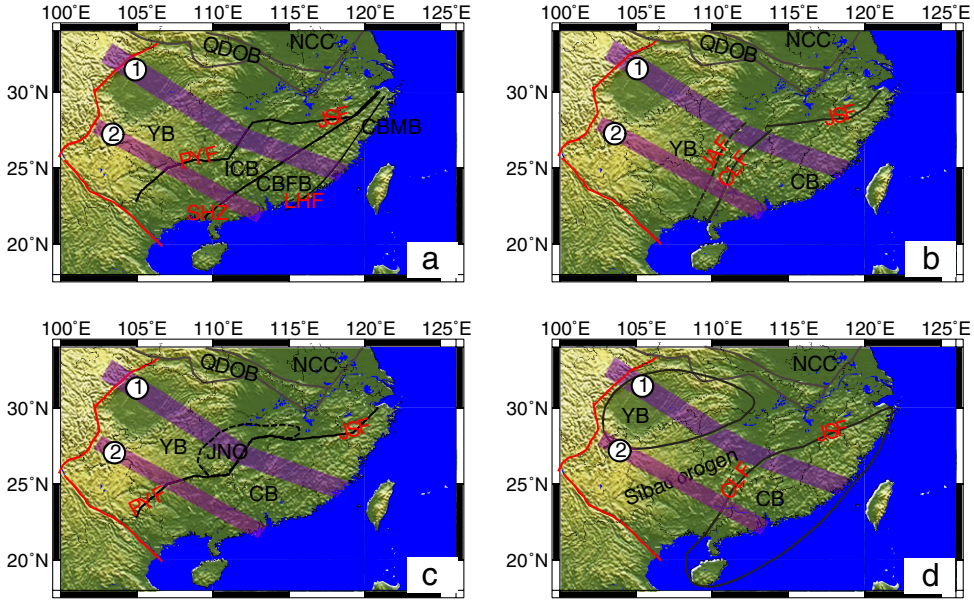

Fig. 8. Four plots showing possible cases wherein the boundaries separate different tectonic units in South China. The blocks are crossed from northwest to southeast by two shading profiles labeled ① and ②, that are the two transects taken as reference later (in Figs. 9 and 10). Key to symbols: NCC, North China Craton; QDOB, Qinling–Dabie orogen belt; YB, Yangtze block; CB, Cathaysia block; ICB, Inner Cathaysia block; CBFB, Cathaysia block fold belt; CBMB, Cathaysia block magmatic belt; JNO, Jiangnan orogen; PYF, Pingxiang–Yushan fault; JAF, Jiangxian–Anhua fault; JSF, Jiangshan–Shaoxing fault; CLF, Chenzhou–Linwu fault; LHF, Lishui–Haifeng fault; SHZ, Shi–Hang zone.

and Jahn, 1998). However, Li et al. (2002, 2008) suggested the South China was formed through the amalgamation of the Yangtze and Cathaysia blocks during the ca. 1.1–0.9 Ga Sibao orogeny (Li and Li, 2007; Li et al., 2002, 2012; Wang et al., 2009), which gave rise to the division of South China into three parts: the Yangtze block, the Cathaysia block and the Sibao orogen (hypothesis proposed in Fig. 8d).

Y.J. Wang et al. (2003) and Wang et al. (2012) have used geochronological and geochemical data to confirm that the Chenzhou–Linwu fault (CLF) represents the Mesozoic lithospheric boundary between the Yangtze and Cathaysia blocks, while the Jinxian–Anhua fault (JAF) is a near-surface boundary between the sutured blocks (hypothesis proposed in Fig. 8b).

The Pingxiang–Yushan fault (PYF) is also considered as the boundary in agreement with geotectonic (Ren et al., 1999) and lithological (Liu et al., 2012) information (hypothesis suggested in Fig. 8c). Alternatively, the Cathaysia block can be separated into Inner Cathaysia Block (ICB), Cathaysia Block Folded Belt (CBFB) and Southeast Coast Magmatic Belt (CBMB) by two tectonic lines, the Shi–Hang Zone (SHZ) and the Lishui–Haifeng Fault (LHF) (Chen et al., 2008) (hypothesis proposed in Fig. 8a). The fact that Triassic granitic rocks (S-type) are mainly distributed in ICB and CBFB, Cretaceous rocks (I-type) in CBMB, and Jurassic rocks (intermediate type) in CBFB, is the basis for Mesozoic tectonic models of Cathaysia (Chen et al., 2008).

Also, the Jiangnan orogen (JNO) is considered as the convergence area between the Yangtze block and the Cathaysia block, thus constituting South China (Wang et al., 2007; Wong et al., 2009) (hypothesis proposed in Fig. 8c).

The way here followed to discern these boundaries is to look into the potential correlation between them and the variations in the geophysical properties of the medium, in our case as gravity, seismic velocity and density. Fig. 9 shows the geophysical data related to profile ① (Fig. 8), namely: topography (a), Bouguer gravity (b), P-wave velocity distribution (d) and density structure (e). As can be seen, the Bouguer gravity increases rapidly from −400 mGal to −100 mGal beside the Longmenshan fault, and its variation curve is roughly flat in the interior of South China. The calculated gravity is similar to the observed gravity, and both curves keep mirror-symmetry with the topography (Fig. 9a,b).

The structures (blocks and faults) along profile ① in the four cases given above (Fig. 8), are indicated in Fig. 9c. The P-wave velocity and density structures allow to observe the thinning from west to east of the crust (Fig. 9d and e) which lies about 45 km beneath Sichuan basin and 30 km beneath the southern margin of the Cathaysia block (Fig. 9e). The Moho interface varies somewhat abruptly beneath the Xuefengshan orogenic belt (Li and Mooney, 1998; Li et al., 2006; Zhang et al., 2010), which is further confirmed by recent deep seismic reflection profiling across the Xuefengshan fault belt, performed in the frame of the Sinoprobe program (Gao, personal communication).

The density in the upper crust of South China is 2.4–2.8 g/cm^3, and 2.9 g/cm^3 in the middle crust, and reaches up to 3.0 g/cm^3 in the lower crust. Sichuan basin has a higher density than any other area in South China, especially in the lower crust, which is consistent with that the Yangtze Craton is the oldest basement in South China (Qiu et al., 2000; Zhang et al., 2009b) (Fig. 9e). Another important feature of the density structure is that the Moho interface is deeper than 40 km to the west of CLF, while it is about 30 km to the east of CLF, and the lower crust is obviously thicker to the east of CLF.

Analogously, Fig. 10 shows the geophysical data related to profile ② (Fig. 8). The difference in topographic relief (elevation) is about 3 km, and the Bouguer gravity increases from −300 mGal to almost 0 mGal. As before, the calculated gravity is similar to the observed gravity, although the former is less curly than the latter, and both curves keep mirror-symmetry with the topography (Fig. 10a,b). The structures (blocks and faults) now crossed by profile ② in the cases (a), (b) and (d) (Fig. 8), are indicated in Fig. 10c. The crustal thickness also shows a west–east thinning and the Moho interface varies laterally from 50 km to 30 km (Fig. 10d). Another important feature is that low-density bodies exist in the Chuandian area, which is consistent with the P-wave velocity determined by deep seismic soundings (Cui et al., 1987; Xiong et al., 1993).

From the two transects, though we cannot accurately appraise the distinctive changes in the geophysical features on both sides of the Chenzhou–Linwu fault because of the relatively large grid interval, the true is that the observed differences in gravity, upper-to-middle crust, thickness of the lower crust, Moho depth, P-wave velocity and density, are all issues which can help to discern the physical boundary between

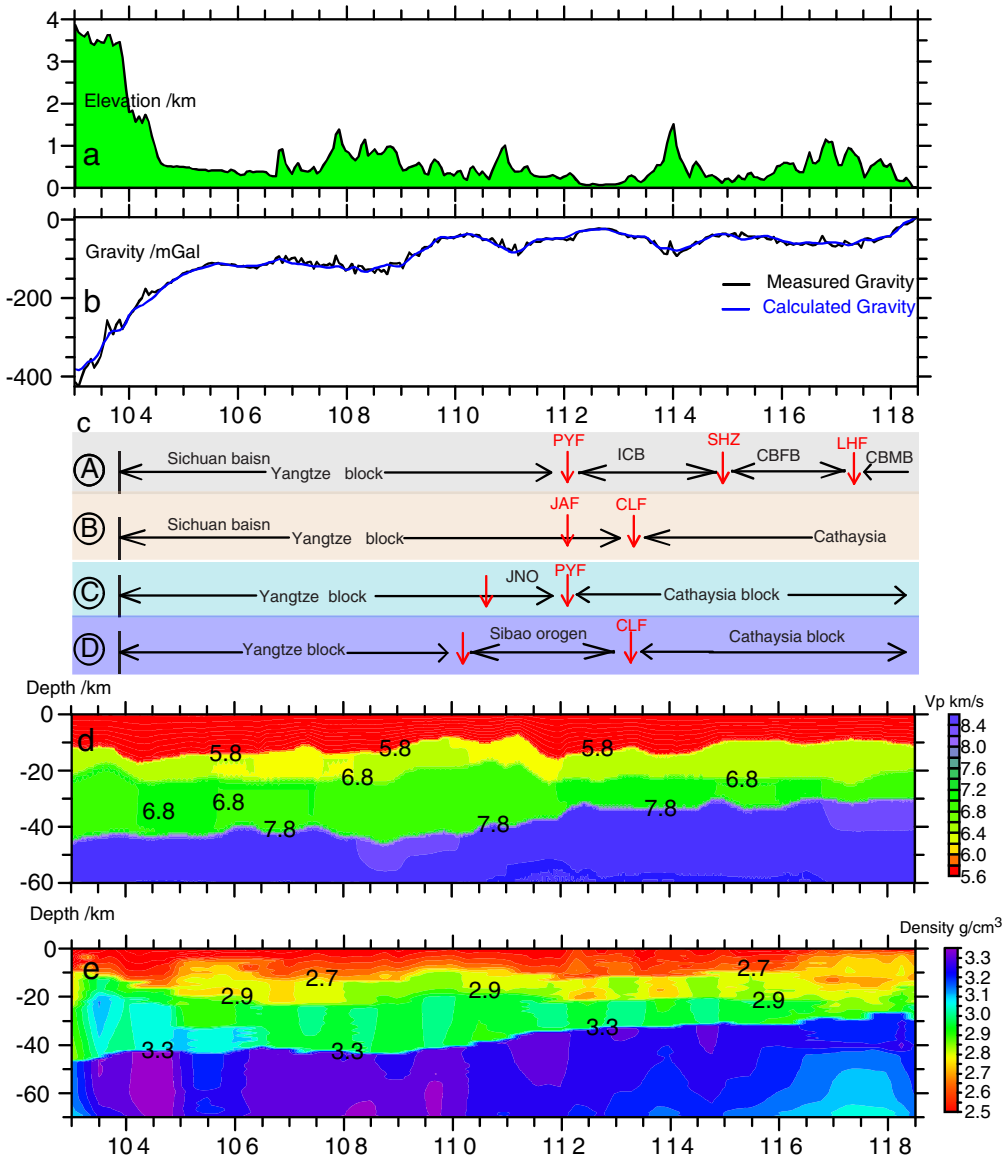

Fig. 9. (a) Topographic relief (elevations) of the profile ① (Fig. 8). (b) Measured and calculated Bouguer gravity anomaly. (c) Testing varying boundaries between blocks (the abbreviations are the same as in Fig. 8). (d) Laterally varying P-wave velocity along the profile ①. (e) Density structure along the profile ①.

blocks. And the geophysical features are not the only ones that reveal remarkable differences near CLF. The region to the east is dominated by structures of the Early Paleozoic with WNW–ESE trending; however, to the west, structures of the Early Mesozoic with NE–SW trend are the most noticeable features (Chen et al., 2008; Chu et al., 2012; Y.J. Wang et al., 2003). Moreover, according to the results from the Lianxian–Gangkou profile (Yin et al., 1999; Zhang et al., 2012), the thickness and average P-wave velocity beneath both of the sedimentary layer and the crystalline basement to the east of CLF are different from that found to the west of this fault (Zhang et al., 2012).

Considering all these factors, though the Pingxiang–Yushan fault also exhibits border features, which just may be the geophysical response to Xuefengshan, the Chenzhou–Linwu fault seems to be the south part of the boundary between the Yangtze and Cathaysia blocks.

4.3. The relationship between P-wave velocity and density

Different mathematical correlations between seismic P-wave velocity and density have been tested by several laboratory works about the elastic properties of crustal rocks. Initially, Ludwig et al. (1970) and Nafe and Drake (1957) performed velocity and density measurements on a variety of rock types thus linked a physical quantity to another. Such a distribution is often interpreted as the natural scatter of velocity values around a mean linear function describing the relationship between seismic velocity and density (Ludwig et al., 1970).

Gardner et al. (1974) found an empirical relationship between density and velocity from a series of field data and controlled laboratory measurements on brine-saturated rocks (excluding evaporates) at several sites and depths. Such relation is given by $\rho = aV^m$ where ρ is density and V is P-wave velocity. Default values for the coefficient a and the exponent m are 0.31 and 0.25, respectively, for density in g/cm^3 and P-wave velocity in m/s.

Somewhat later, Barton (1986) established bounds for this relationship, such as shown in Fig. 11, where the red continuous lines represent the P-wave velocity curves corresponding to the maximum and minimum values of density, while the red dashed line in the center of the scatter corresponds to the mean density value.

Moreover, petrophysical analyses have proved that bulk density is an important acoustic indicator to discern rock types (Christensen and Mooney, 1995; Quijada and Stewart, 2007; Zhang et al., 2008).

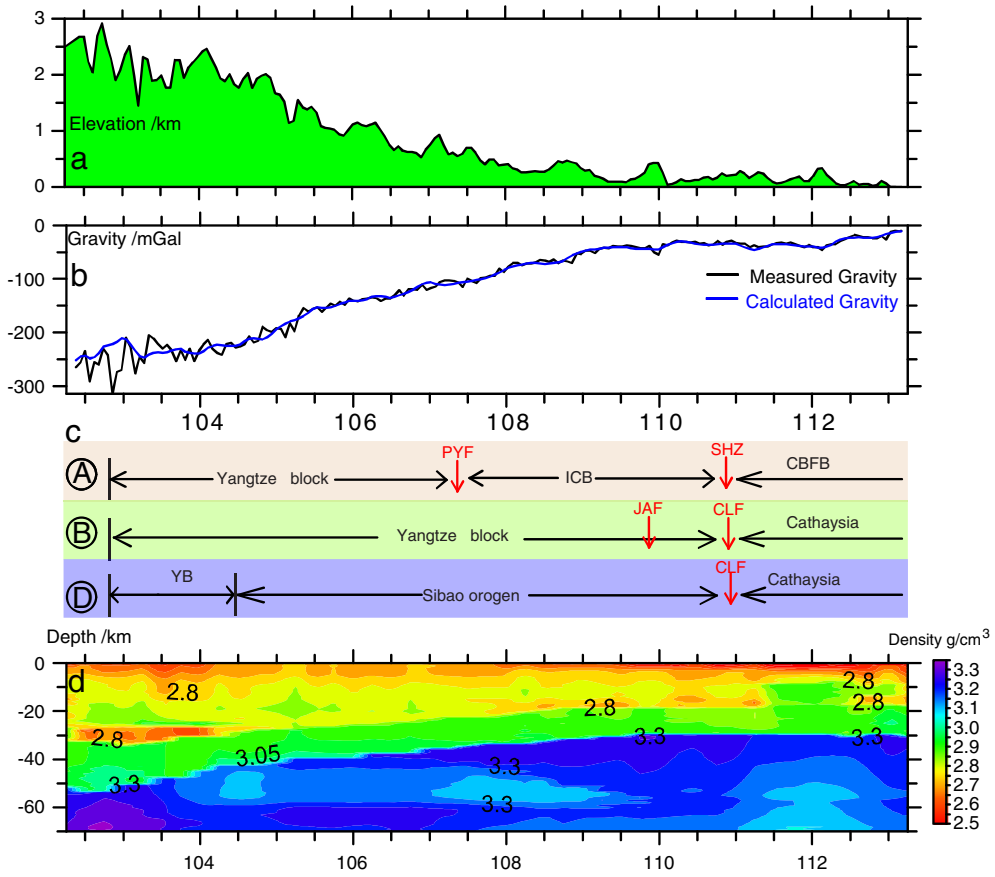

Fig. 10. (a) Topographic relief (elevations) of the profile ② (Fig. 8). (b) Measured and calculated Bouguer gravity anomaly. (c) Testing varying boundaries between blocks (the abbreviations are the same as in Fig. 8). (d) Density structure along the profile ②.

In this study, we start from the velocity–density reference model given by Eqs. (1)–(3), which is confirmed as a more valid relationship for the determination of crustal density in China (Feng et al., 1986; Zhao et al, 2004; Wang et al., 2010). The scattered Vp–density relationship is obtained through an inversion process and plotted by a point cloud for the main tectonic units that make up the study region (Fig. 11). Subsequently, it is modeled by least-squares linear regression with the results: $y = 4.45 * x - 6.28$ in Qinling–Dabie Orogen, $y = 3.89 * x - 4.77$ in Sichuan basin, $y = 4.54 * x - 6.46$ in Cathaysia block and $y = 4.16 * x - 5.49$ in Yangtze block. It should be noted that the method is designed to incorporate the main scatter of the measurements with the exclusion of peripheral values. The most remarkable feature is that the inverted density is not the same as the initial one, from which diverges within the range of lower values. The slope of the regression straight for Sichuan basin takes the smallest value, which means that for a same P-wave velocity we have the highest density, while the opposite happens in Cathaysia block, where the slope takes the comparatively larger value and for a same P-wave velocity we have the lowest density. The possible explanation of these results can be attributed to the temperature, pressure and composition of each tectonic area (Christensen and Mooney, 1995). The Sichuan basin is an old craton that has preserved its rigidity for a long time, and its crustal composition is different from that any other region (T. Xu et al., 2010; Y. Xu et al., 2010; Zhang et al., 2010), so this could be the reason for the higher resulting density; while in the Cathaysia block the strong neotectonic movement cause the heat flow and geothermal gradient be relatively higher than in other region (Deng et al., 2013; Hu et al., 2001; Tao and Shen, 2008), so the crustal temperature is higher and hence the corresponding density is relatively lower.

Undoubtedly, estimating the composition of the Earth's crust is important because such knowledge is critical to understand the growth and evolution of the continents (Brown et al., 2003; Holbrook et al., 1999; Zhang et al., 2008). Although investigating rock types based on its lithological composition is out of the target of this paper, we think that the established Vp–density laws for the major tectonic domains of South China will help to address this problem in future. And this issue has already been thoroughly addressed by our working group (Zhang et al., 2008, X. Zhang et al., 2011; Zhao et al., 2013b). In this context, seismic velocity and density play a key role since they are inherent properties of rock types (Christensen and Mooney, 1995), so that combined interpretations of both can be widely used to infer lithological models.

5. Conclusions

In contrast to most of the previous geophysical studies, which focus on individual linear profiles crossing different tectonic units in South China and only reveal 2-D crustal structures, in this paper we have tackled a 3-D inversion process constrained by seismic velocities and gravity data. Key findings include:

(1) We have obtained a regional density model which is consistent with complementary data supplied by other studies. From here we can accurately reproduce the observed gravity field.
(2) The Moho depth can be drawn from the inverted density structure and agrees with the results from wide-angle reflection/refraction profiles. The crustal thickness shows a gradual thinning west-to-east from 45–50 km to 30 km.

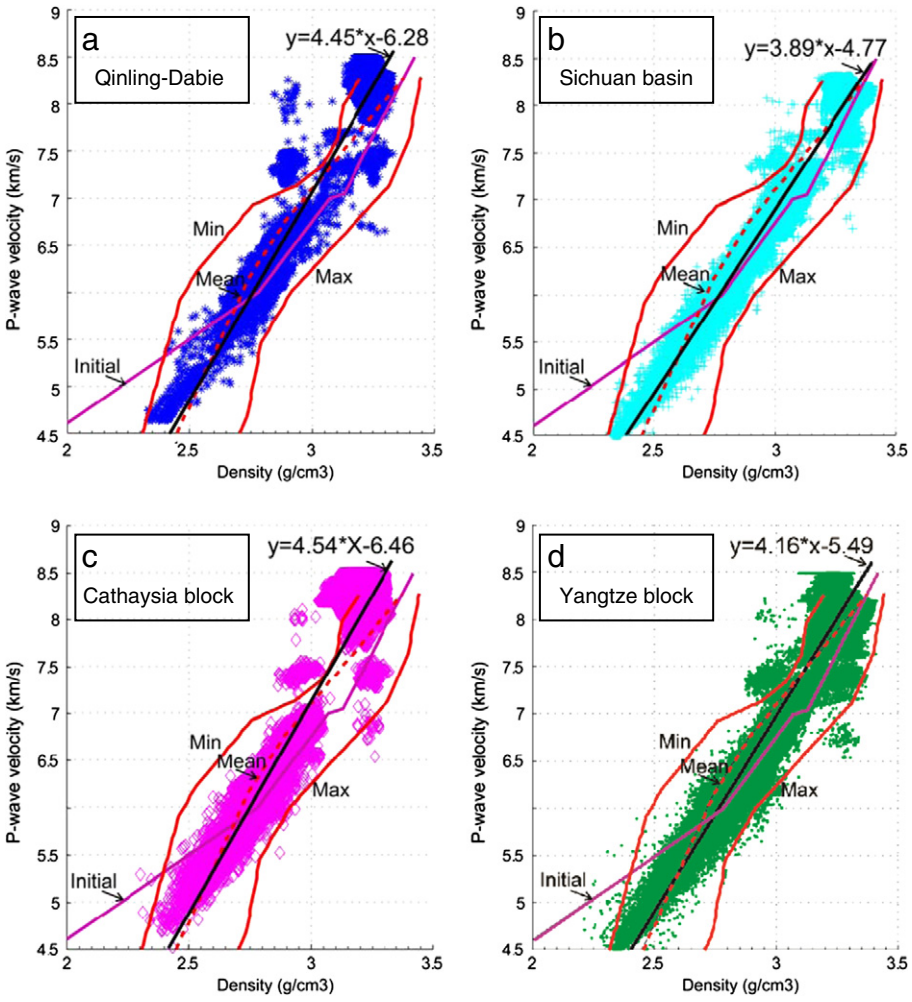

Fig. 11. The relationship between P-wave velocity and density (after zonation): (a) Qinling–Dabie; (b) Sichuan basin; (c) Cathaysia block; (d) Yangtze block. The red continuous lines represent the P-wave velocity curves corresponding to the maximum and minimum values of density, while the red dashed line in the center of the scatter corresponds to the mean density value (according to Barton, 1986). The purple line depicts the initial relationship between Vp and density. The scattered Vp–density relationship is plotted by a point cloud for the main tectonic units that make up the study region and is modeled by least-squares regression (black straight line), whose analytical expression is given on the top of each plot.

(3) Regardless the existence of a low-density layer in the 10–20 km depth range, a linearly increasing density consistent with a high P-wave velocity supports the presence of the speculated buried dome in east of the Dabie orogen, as deep seismic soundings reported clearly before. This geophysical feature is viewed as a fossil rest of the collision/extrusion between the North China Craton and the Yangtze Craton.

(4) Once combined all geophysical and geological data, we propose that the Chenzhou–Linwu fault is the south segment of the boundary between the Yangtze and Cathaysia blocks.

(5) By least-squares linear regression we have modeled four Vp–density laws, in correspondence with the main tectonic units that make up South China. These linear relationships between P-wave velocity and density present different slope in each of these large areas, which is attributed to the crustal composition and temperature distribution.

Acknowledgments

We are grateful to the University of British Columbia, Canada, for providing us the software Grav3D. We appreciate the constructive suggestions on the interpretation of geodynamic processes made by Yuejun Wang. The helpful comments made by anonymous reviewers helped to improve the manuscript greatly. The Ministry of Science and Technology of China (Sinoprobe-03-02, Sinoprobe-02-02) and the National Nature Science Foundation of China (grants 41021063, 41274090, 41004017) supported financially this study.

References

Bai, Z.M., Zhang, Z.J., Wang, Y.H., 2007. Crustal structure across the Dabie-Sulu orogenic belt revealed by seismic velocity profiles. Journal of Geophysics and Engineering 4 (4), 436–442.

Barton, P., 1986. The relationship between seismic velocity and density in the continental crust—a useful constraint? Geophysical Journal International 87 (1), 195–208.

Brown, D., Carbonell, R., Kukkonen, I., Ayala, C., Golovanova, I., 2003. Composition of the Uralide crust from seismic velocity (Vp, Vs), heat flow, gravity, and magnetic data. Earth and Planetary Science Letters 210 (1), 333–349.

Cella, F., Fedi, M., Florio, G., Grimaldi, M., Rapolla, A., 2007. Shallow structure of the Somma–Vesuvius volcano from 3D inversion of gravity data. Journal of Volcanology and Geothermal Research 161 (4), 303–317.

Chen, J., Jahn, B.-m., 1998. Crustal evolution of southeastern China: Nd and Sr isotopic evidence. Tectonophysics 284, 101–133.

Chen, C.H., Lee, C.Y., Shinjo, R., 2008. Was there Jurassic paleo-Pacific subduction in South China?: constraints from $^{40}Ar/^{39}Ar$ dating, elemental and Sr–Nd–Pb isotopic geochemistry of the Mesozoic basalts. Lithos 106, 83–92.

Christensen, N.I., Mooney, W.D., 1995. Seismic velocity structure and composition of the continental crust: a global view. Journal of Geophysical Research 100 (B6), 9761–9788.

Chu, Y., Lin, W., Faure, M., Wang, Q., Ji, W., 2012. Phanerozoic tectonothermal events of the Xuefengshan Belt, central South China: implications from U–Pb age and Lu–Hf determinations of granites. Lithos 150, 243–255.

Cui, Z.Z., Lu, D.Y., Chen, J.P., Zhang, Z.Y., Huang, L.Y., 1987. The deep structural and tectonic features of the crust in panxi area. Chinese Journal of Geophysics (Acta Geophysica Sinica) 30 (6), 566–580 (in Chinese with abstract in English).
Cui, Z.Z., Chen, J.P., Wu, L., 1996. Memoirs of the Geoscience Transection for the Continental Lithosphere beneath Altay—Taiwan. Geological Press, Beijing.
Deng, Y.F., Li, S.L., Fan, W.M., Liu, J., 2011. Crustal structure beneath South China revealed by deep seismic soundings and its dynamics implications. Chinese Journal of Geophysics 54 (10), 2560–2574 (in Chinese with abstract in English).
Deng, Y., Fan, W., Zhang, Z., Badal, J., 2012. Geophysical evidence on segmentation of the Tancheng–Lujiang fault and its implications on the lithosphere evolution in East China. Journal of Asian Earth Sciences. http://dx.doi.org/10.1016/j.jseaes.2012.1011.1006.
Deng, Y., Zhang, Z., Fan, W., Pérez-Gussinyé, M., 2013. Multitaper spectral method to estimate the elastic thickness of South China and its implications for intracontinental deformation. Geoscience Frontiers. http://dx.doi.org/10.1016/j.gsf.2013.1005.1002.
Dong, S.W., Wu, X.Z., Gao, R., Lu, D.Y., Li, Y.K., He, Y.Q., Tang, J.F., Cao, F.Y., Hou, M.J., Huang, D.Z., 1998. On the crust velocity levels and dynamics of the Dabieshan orogenic belt. Chinese Journal of Geophysics 41 (3), 349–361 (in Chinese with abstract in English).
Dutra, A.C., Marangoni, Y.R., 2009. Gravity and magnetic 3D inversion of Morro do Engenho complex, Central Brazil. Journal of South American Earth Sciences 28 (2), 193–203.
Feng, R., Yan, H.F., Zhang, R.S., 1986. Fast inversion method and corresponding programming for 3D potential field. Acta Geologica Sinica 4 (3), 390–402 (in Chinese with abstract in English).
Gardner, G., Gardner, L., Gregory, A., 1974. Formation velocity and density—the diagnostic basics for stratigraphic traps. Geophysics 39 (6), 770–780.
Granitoid Research Group of the Nanling Project, 1989. Geology of Granitoids of Naling Region and Their Petrogenesis and Mineralization. Geological Publishing House, Beijing.
GRAV3D, 2005. A Program Library for Forward Modelling and Inversion of Gravity Data Over 3D Structures, Version 3.0. UBC—Geophysical Inversion Facility, Department of Earth and Ocean Sciences, University of British Columbia, Vancouver, British Columbia.
Hirajima, T., Nakamura, D., 2003. The Dabie Shan–Sulu orogen. Ultrahigh Pressure Metamorphism 5, 105–144.
Holbrook, W.S., Lizarralde, D., McGeary, S., Bangs, N., Diebold, J., 1999. Structure and composition of the Aleutian island arc and implications for continental crustal growth. Geology 27 (1), 31–34.
Hu, S.B., He, L.J., Wang, J.Y., 2001. Compilation of heat flow data in the China continental area. Chinese Journal of Geophysics 44 (5), 604–618.
Huang, C., 1977. Basic features of the tectonic structure of China. International Geology Review 5, 289–302.
Huang, J., Zhao, D., 2006. High-resolution mantle tomography of China and surrounding regions. Journal of Geophysical Research 111 (B9), B09305.
Ji, X., Coney, P.J., 1985. Accreted terranes in China. Howell, D.G. (Ed.), Tectonostratigraphic Terranes of the Circum-Pacific Region, Earth Sci. Ser., vol. 1. Circum-Pac. Counc. Energ. Miner. Resour, Houston, Tex, pp. 349–361.
Li, J., 1992. Study on Structure and Evolution of Oceanic–Continental Lithosphere in Southeast China. Science and Technology Press of China, Beijing.
Li, Z.X., 1994. Collision between the North and South China blocks: a crustal-detachment model for suturing in the region east of the Tanlu fault. Geology 22 (8), 739.
Li, Z.X., Li, X.H., 2007. Formation of the 1300-km-wide intracontinental orogen and postorogenic magmatic province in Mesozoic South China: a flat-slab subduction model. Geology 35, 179–182.
Li, S.L., Mooney, W.D., 1998. Crustal structure of China from deep seismic sounding profiles. Tectonophysics 288, 105–114.
Li, Y., Oldenburg, D.W., 1996. 3-D inversion of magnetic data. Geophysics 61 (2), 394–408.
Li, Y., Oldenburg, D.W., 1998. 3-D inversion of gravity data. Geophysics 63 (1), 109–119.
Li, Y., Yang, Y., 2011. Gravity data inversion for the lithospheric density structure beneath North China Craton from EGM 2008 model. Physics of the Earth and Planetary Interiors 189 (1–2), 9–26.
Li, S., Xiao, Y., Liou, D., Chen, Y., Ge, N., Zhang, Z., Sun, S., Cong, B., Zhang, R., Hart, S.R., 1993. Collision of the North China and Yangtse Blocks and formation of coesite-bearing eclogites: timing and processes. Chemical Geology 109 (1–4), 89–111.
Li, Z.X., Li, X., Zhou, H., Kinny, P.D., 2002. Grenvillian continental collision in south China: new SHRIMP U–Pb zircon results and implications for the configuration of Rodinia. Geology 30, 163–166.
Li, S.L., Mooney, W.D., Fan, J.C., 2006. Crustal structure of mainland China from deep seismic sounding data. Tectonophysics 420, 239–252.
Li, Z., Li, X., Li, W., Ding, S., 2008. Was Cathaysia part of Proterozoic Laurentia? -new data from Hainan Island, south China. Terra Nova 20, 154–164.
Li, Z.X., Li, X.H., Chung, S.L., Lo, C.H., Xu, X., Li, W.X., 2012. Magmatic switch-on and switch-off along the South China continental margin since the Permian: transition from an Andean-type to a Western Pacific-type plate boundary. Tectonophysics 532–535, 271–290.
Liu, F.T., Xu, P.F., Liu, J.S., Yin, Z.X., Qin, J.Y., Zhang, X.K., Zhang, C.K., Zhao, J.R., 2003. The crustal velocity structure of the continental deep subduction belt: study on the eastern Dabie orogen by seismic wide-angle reflection/refraction. Chinese Journal of Geophysics 46 (3), 366–372 (in Chinese with abstract in English).
Liu, Y., Li, S., Xu, S., Jahn, B.-M., Zheng, Y.-F., Zhang, Z., Jiang, L., Chen, G., Wu, W., 2005. Geochemistry and geochronology of eclogites from the northern Dabie Mountains, central China. Journal of Asian Earth Sciences 25 (3), 431–443.
Liu, C.Z., Liu, Z.C., Wu, F.Y., Chu, Z.Y., 2012. Mesozoic accretion of juvenile sub-continental lithospheric mantle beneath South China and its implications: geochemical and Re–Os isotopic results from Ningyuan mantle xenoliths. Chemical Geology 291, 186–198.
Ludwig, W.J., Nafe, J.E., Drake, C.L., 1970. Seismic refraction. The Sea 4, 53–84.
Luo, Y., Xu, Y., Yang, Y., 2012. Crustal structure beneath the Dabie orogenic belt from ambient noise tomography. Earth and Planetary Science Letters 313–314, 12–22.
Ma, Y., Zhou, H., 2007. Crustal thicknesses and Poisson's ratios in China by joint analysis of inearized receiver functions and Rayleigh wave dispersion. Geophysical Research Letters 34, L12304. http://dx.doi.org/10.1029/2007GL029848.
Mooney, W.D., Kaban, M.K., 2010. The North American upper mantle: density, composition, and evolution. Journal of Geophysical Research 115 (B12), B12424.
Nafe, J.E., Drake, C.L., 1957. Variation with depth in shallow and deep water marine sediments of porosity, density and the velocities of compressional and shear waves. Geophysics 22 (3), 523–552.
Okay, A.I., 1993. Petrology of a diamond and coesite-bearing metamorphic terrain: Dabie Shan, China. European Journal of Mineralogy 5, 659–675.
Pavlis, N.K., Holmes, S.A., Kenyon, S.C., Factor, J.K., 2008. An earth gravitational model to degree 2160: EGM2008. EGU General Assembly 13–18.
Pavlis, N.K., Holmes, S.A., Kenyon, S.C., Factor, J.K., 2012. The development and evaluation of the Earth Gravitational Model 2008 (EGM2008). Journal of Geophysical Research 117 (B4), B04406.
Qiu, Y., Gao, S., McNaughton, N., Groves, D., Ling, W., 2000. First evidence of >3.2 Ga continental crust in the Yangtze craton of South China and its implications for Archean crustal evolution and Phanerozoic tectonics. Geology 28, 11–14.
Quijada, M.F., Stewart, R.R., 2007. Density estimations using density–velocity relations and seismic inversion. CREWES Research Report 19, 1–20.
Ren, J.S., Wang, Z.X., Chen, B.W., 1999. View on China Tectonics From Globe: Brief Introduction of the Tectonic Map of China and Adjacent Area. Geological Publishing House, Beijing 1–50.
Tao, W., Shen, Z., 2008. Heat flow distribution in Chinese continent and its adjacent areas. Progress in Natural Science 18 (7), 843–850.
Teng, J.W., 2003. Introduction to Solid Geophysics. Seismological Press, Beijing.
Wang, J.Y., 2002. Inverse Theory in Geophysics. Higher Education Press Beijing.
Wang, Q.C., 2009. Preliminary discuss ion on sedimentary tectonics of the clustered continents of South China. Acta Sedimentological Sinica 27 (5), 811–817 (in Chinese with abstract in English).
Wang, H.Z., Qiao, X.F., 1984. Proterozoic stratigraphy and tectonic framework of China. Geological Magazine 121, 599–614.
Wang, D., Shu, L., 2012. Late Mesozoic basin and range tectonics and related magmatism in Southeast China. Geoscience Frontiers 3 (2), 109–124.
Wang, C., Chan, W., Mooney, W.D., 2003. Three-dimensional velocity structure of crust and upper mantle in southwestern China and its tectonic implications. Journal of Geophysical Research 108. http://dx.doi.org/10.1029/2002JB001973.
Wang, Q.S., An, Y.L., Zhang, C.J., Jiang, F.Z., 2003. Gravitology. Seismological Press, Beijing 17–33.
Wang, Y.J., Fan, W.M., Guo, F., Peng, T., Li, C., 2003. Geochemistry of Mesozoic mafic rocks adjacent to the Chenzhou–Linwu fault, South China: implications for the lithospheric boundary between the Yangtze and Cathaysia blocks. International Geology Review 45, 263–286.
Wang, X.-L., Zhou, J.-C., Griffin, W., Wang, R.-C., Qiu, J.-S., O'Reilly, S., Xu, X., Liu, X.-M., Zhang, G.-L., 2007. Detrital zircon geochronology of Precambrian basement sequences in the Jiangnan orogen: Dating the assembly of the Yangtze and Cathaysia Blocks. Precambrian Research 159, 117–131.
Wang, X.C., Li, X.H., Li, W.X., Li, Z.X., 2009. Variable involvements of mantle plumes in the genesis of mid-Neoproterozoic basaltic rocks in South China: a review. Gondwana Research 15, 381–395.
Wang, Q.S., Teng, J.W., An, Y.L., Zhang, Y.Q., 2010. Gravity field and deep crustal structures of the Yinshan orogen and the northern Ordos basin. Progress in Geophysics 25 (5), 1590–1598 (in Chinese with English abstract).
Wang, Y., Wu, C., Zhang, A., Fan, W., Zhang, Y., Zhang, Y., Peng, T., Yin, C., 2012. Kwangsian and Indosinian reworking of the eastern South China Block: constraints on zircon U–Pb geochronology and metamorphism of amphibolites and granulites. Lithos 150, 227–242.
Welford, J.K., Hall, J., 2007. Crustal structure of the Newfoundland rifted continental margin from constrained 3-D gravity inversion. Geophysical Journal International 171 (2), 890–908.
Welford, J.K., Shannon, P.M., O'Reilly, B.M., Hall, J., 2010. Lithospheric density variations and Moho structure of the Irish Atlantic continental margin from constrained 3-D gravity inversion. Geophysical Journal International 183, 79–95.
Wong, J., Sun, M., Xing, G., Li, X., Zhao, G., Wong, K., Yuan, C., Xia, X., Li, L., Wu, F., 2009. Geochemical and zircon U–Pb and Hf isotopic study of the Baijuhuajian metaluminous A-type granite: extension at 125–100 Ma and its tectonic significance for South China. Lithos 112, 289–305.
Xiong, S.B., Zheng, Y., Yin, Z.X., Zeng, X.X., Quan, Y.L., Sun, K.Z., 1993. The 2-D structure and it's tectonic implications of the crust in the Lijiang–Panzhihua–Zhehai region. Chinese Journal of Geophysics (Acta Geophysica Sinica) 36 (4), 434–444 (in Chinese with abstract in English).
Xiong, X.S., Gao, R., Li, Q.S., Lu, Z.W., Wang, H.Y., Li, W.H., Guan, Y., 2009. The Moho depth of South China revealed by seismic probing. Acta Geoscientica Sinica 30 (6), 774–786 (in Chinese with abstract in English).
Xu, T., Zhang, Z., Gao, E., Xu, G., Sun, L., 2010. Segmentally iterative ray tracing in complex 2D and 3D heterogeneous block models. Bulletin of the Seismological Society of America 100 (2), 841–850.
Xu, Y., Li, Z.W., Huang, R.Q., Huang, R.Q., Liu, J.H., Liu, J.S., 2010. Pn wave velocity and anisotropy in the west of Sichuan and Longmenshan. Science in China (Series D) 40 (4), 452–457 (in Chinese).
Yin, Z.X., Lai, M.H., Xiong, S.B., Liu, H.B., Teng, J.W., Kong, X.R., 1999. Crustal structure and velocity distribution from deep seismic sounding along the profile of Lianxian-Boluo-Gangkou in South China. Chinese Journal of Geophysics 42 (3), 383–392 (in Chinese with English abstract).
Zeng, H.L., 2005. Gravity Field and Gravity Exploration. Geological Publishing House, Beijing 79–100.

Zhang, Z.J., Wang, Y., 2007. Crustal structure and contact relationship revealed from deep seismic sounding data in South China. Physics of the Earth and Planetary Interiors 165 (1–2), 114–126.
Zhang, Z.M., Liou, J.G., Coleman, R.G., 1984. An outline of the plate tectonics of China. Geological Society of America Bulletin 95 (3), 295–312.
Zhang, Z.J., Badal, J., Li, Y., Chen, Y., Yang, L., Teng, J., 2005. Crust–upper mantle seismic velocity structure across Southeastern China. Tectonophysics 395 (1), 137–157.
Zhang, Z.J., Zhang, X., Badal, J., 2008. Composition of the crust beneath southeastern China derived from an integrated geophysical data set. Journal of Geophysical Research 113 (B4), B04417.
Zhang, Z.J., Teng, J., Badal, J., Liu, E., 2009a. Construction of regional and local seismic anisotropic structures from wide-angle seismic data: crustal deformation in the southeast of China. Journal of Seismology 13 (2), 241–252.
Zhang, Z.J., Zhao, B., Zhang, X., Teng, J., 2009b. Crustal wide-angle reflection imaging along Lianxian–Gangkou profile in Guangdong province, China. Earthquake Science 22 (4), 357–363.
Zhang, Z.J., Bai, Z.M., Mooney, W., Wang, C.Y., Chen, X.B., Wang, E.C., Teng, J.W., Okaya, N., 2009c. Crustal structure across the three Gorges area of the Yangtze platform, central China, from seismic refraction/wide-angle reflection data. Tectonophysics 475 (3–4), 423–437.
Zhang, Z.J., Yuan, X.H., Chen, Y., Tian, X.B., Kind, R., Li, X., Teng, J.W., 2010. Seismic signature of the collision between the east Tibetan escape flow and the Sichuan Basin. Earth and Planetary Science Letters 292 (3–4), 254–264.
Zhang, X., Brown, D., Deng, Y., 2011. Crustal composition model across the Bangong–Nujiang suture belt derived from INDEPTH III velocity data. Journal of Geophysics and Engineering 8 (4), 549–559.
Zhang, Z.J., Yang, L.Q., Teng, J.W., Badal, J., 2011. An overview of the earth crust under China. Earth-Science Reviews 104 (1–3), 143–166. http://dx.doi.org/10.1016/j.earscirev.2010.10.003.
Zhang, Z.J., Xu, T., Zhao, B., Badal, J., 2012. Systematic variations in seismic velocity and reflection in the crust of Cathaysia: new constraints on intraplate orogeny in the South China continent. Gondwana Research. http://dx.doi.org/10.1016/j.gr.2012.05.018.
Zhang, Z.J., Deng, Y.F., Chen, L., Wu, J., Teng, J.W., Panza, G., 2013. Seismic structure and the rheology of the crust beneath mainland China. Gondwana Research 23 (4), 1455–1483. http://dx.doi.org/10.1016/j.gr.2012.07.010.
Zhao, J.M., Li, Z.C., Cheng, H.G., Yao, C.L., Li, Y.S., 2004. Structure of lithospheric density and geomagnetism beneath the Tianshan orogenic belt and their geodynamic implications. Chinese Journal of Geophysics 47 (6), 1061–1067 (in Chinese with abstract in English).
Zhao, B., Zhang, Z., Bai, Z., Badal, J., Zhang, Z., 2013a. Shear velocity and Vp/Vs ratio structure of the crust beneath the southern margin of South China continent. Journal of Asian Earth Sciences 62, 167–179. http://dx.doi.org/10.1016/j.jseaes.2012.08.013.
Zhao, B., Bai, Z., Xu, T., Zhang, Z., Badal, J., 2013b. Lithological model of the South China crust based on integrated geophysical data. Journal of Geophysics and Engineering 10. http://dx.doi.org/10.1088/1742-2132/10/2/025005.
Zheng, Y.F., 2008. A perspective view on ultrahigh-pressure metamorphism and continental collision in the Dabie–Sulu orogenic belt. Chinese Science Bulletin 53, 3081–3104.
Zheng, Y.F., Fu, B., Gong, B., Li, L., 2003. Stable isotope geochemistry of ultrahigh pressure metamorphic rocks from the Dabie–Sulu orogen in China: implications for geodynamics and fluid regime. Earth-Science Reviews 62, 105–161.
Zheng, S., Sun, X., Song, X., Yang, Y., Ritzwoller, M.H., 2008. Surface wave tomography of China from ambient seismic noise correlation. Geochemical Geophysical Geosystems 9. http://dx.doi.org/10.1029/2008GC001981.